Macromolecules
ARTICLE

Macromolecules **2009**, *42*, 6075–6085 **6075**
DOI: 10.1021/ma901272s

Highly Selective Polymer Electrolyte Membranes from Reactive Block Polymers

Liang Chen,[†] Daniel T. Hallinan, Jr.,[‡] Yossef A. Elabd,*[,‡] and Marc A. Hillmyer*[,†]

[†]*Department of Chemistry, University of Minnesota, Minneapolis, Minnesota 55455, and* [‡]*Department of Chemical and Biological Engineering, Drexel University, Philadelphia, Pennsylvania 19104*

Received June 12, 2009; Revised Manuscript Received July 1, 2009

ABSTRACT: A series of reactive poly(norbornenylethylstyrene-*s*-styrene)-poly(*n*-propyl-*p*-styrenesulfonate) (PNS−PSSP) block polymers were prepared by atom transfer radical polymerization. Solutions containing PNS−PSSP, the cyclic olefins dicyclopentadiene and/or cyclooctene, and the second-generation Grubbs metathesis catalyst were prepared, cast as thin films, and allowed to cure at room temperature by a ring-opening metathesis polymerization mechanism. Small-angle X-ray scattering (SAXS) data on cured films were consistent with the formation of nanostructured materials containing PSSP domains confined in a cross-linked matrix of the metathesis-reactive PNS block and the poly(cyclic olefins). The PSSP phase in these films was converted into the sulfonic acid form by hydrolysis of the propyl sulfonate ester. The resulting cross-linked polymer electrolyte membranes (PEMs) were characterized by SAXS and transmission electron microscopy. A bicontinuous morphology with continuous domains of the sulfonic acid phase supported by a continuous and mechanically robust phase was evident in these films. The molecular weight of the PNS−PSSP block polymer controlled the domain sizes, and the mechanical properties of the membranes could be tuned through the choice of cyclic olefins used. The PEMs exhibited pronounced mechanical and thermal robustness. Furthermore, proton conductivities in all the PEMs were similar to those observed in Nafion (the most frequently used PEM in fuel cells) at high humidity. Select PEMs showed significantly lower methanol crossover than Nafion while maintaining high-saturated proton conductivities, which could result in higher direct methanol fuel cell power densities. This reactive block polymer strategy for the preparation of PEMs is attractive due to the ready formation of bicontinuous structures, the facile control of domain size, and the ability to independently control mechanical and swelling properties of the matrix material.

Introduction

Fuel cells are promising alternative energy delivery devices capable of highly efficient chemical energy conversions for a range of practical applications spanning portable electronic to automotive technologies.[1] Direct methanol fuel cells (DMFCs), in particular, have received a great deal of attention[2] as alternatives to lithium ion rechargeable batteries due to their high power densities, sustainable nature,[3] and the convenient nature of the liquid fuel (i.e., for instant recharge). A key component of fuel cells is the polymer electrolyte membrane (PEM) that separates the anodic and cathodic reactions while simultaneously allowing proton transfer.[4]

Currently, Nafion, a perfluorinated ionomer, is the benchmark PEM for the DMFC due to its high proton conductivity and excellent chemical, oxidative, and mechanical stabilities.[5] The high proton conductivity of Nafion has been attributed to its ionic structure in the fully hydrated state. Although various morphological models for Nafion have been presented, a phase-segregated morphology with continuous ionic domains is well accepted. For example, Hsu and Gierke[6a] proposed a morphology with ionic clusters less than 5 nm in size contained in the perfluorinated matrix linked by narrow ionic channels of about 1 nm in diameter.[6] The bicontinuity of this morphology is important for the performance of Nafion; the continuous ionic structure allows for proton conductivity, and the continuous matrix provides ample mechanical support. However, the use of Nafion in DMFCs has generally limited overall efficiencies to ∼20−25% and feed concentrations to ∼1−2 M methanol due to methanol crossover (high methanol permeability in Nafion).[7] If PEMs with high proton conductivity and low methanol crossover could be developed, then higher methanol concentrations could be used (e.g., ∼18 M; the ideal equimolar half cell reaction in the DMFC), resulting in significantly higher DMFC efficiencies and power densities.

Many efforts to design alternatives to Nafion have been reported, and this area has been extensively reviewed over the past decade.[8] Some key examples of sulfonated homopolymers include sulfonated polystyrene (SPS),[9] polyimides,[10] polyphosphazenes,[11] polybenzimidazoles,[12] poly(phenylene sulfone)s,[13] poly(arylene ether)s,[14] and aromatic copolymers.[15] In all of the aforementioned sulfonated membranes, the ionic nanostructures were, in general, poorly controlled.

Over the past several years, nanostructured PEMs produced from block and graft copolymers containing SPS have been extensively studied. Self-assembled block copolymers can lead to well-defined nanostructures where the morphology and domain size are tunable on the nanoscopic length scale.[16] More importantly, the physical attributes of the resultant materials can be independently tailored in many cases. For example, grafting SPS onto a fluorinated polymer using radiation-mediated polymerizations,[17] chemical grafting of SPS on PS,[18] poly(arylene ether),[19] poly(ethylene-*co*-tetrafluoroethylene),[20] poly(vinylidene difluoride),[21] and poly(vinylidene difluoride−chlorotrifluoroethylene)[22] have all been explored. Studies of these graft copolymer membranes presented compelling evidence that ionic

*To whom correspondence should be addressed. E-mail: elabd@drexel.edu (Y.A.E.); hillmyer@umn.edu (M.A.H.).

Published on Web 07/27/2009

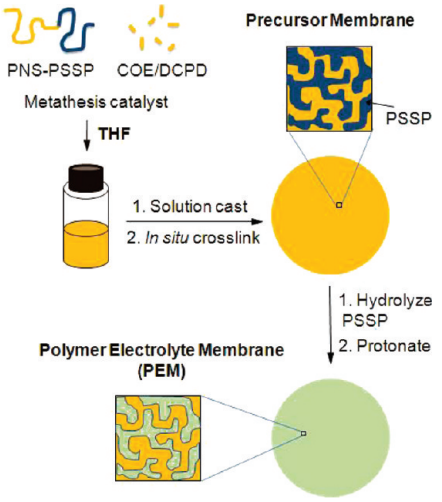

Figure 1. Preparation of a cross-linked polymer electrolyte membrane (PEM) from PNS−PSSP and COE/DCPD by ring-opening metathesis polymerization-induced phase separation.

conductivity was significantly enhanced by forming continuous nanochannels of polyelectrolyte in the matrix material; proton conductivity of all these membranes was an order of magnitude higher than that of SPS, a material that exhibited no clear nanostructure at similar ionic contents.

Studies on other block polymers, such as sulfonated PS-*b*-poly(ethylene-*s*-butene)-*b*-PS,[23] sulfonated PS-*b*-polyisobutene-(PIB)-*b*-PS,[24] poly(ethylene-*s*-styrene) with short alternating sulfonted PS segments,[25] and poly(vinylidene difluoride−hexafluoropropylene)-*b*-SPS[26] have also indicated that the orientation of ionic domains in the PEM membrane could have a significant effect on the proton conductivity; the copolymer composition and the membrane preparation conditions are critically important in this regard. For example, Park et al.[27] studied a series of poly(methylbutylene) (PMB)-*b*-SPS diblock polymers and showed that the bicontinuous morphologies like gyroid or perforated lamellae benefited the proton conductivity. Moreover, they clearly demonstrated that the domain sizes formed by the SPS block played a critical role in preventing membrane dehydration at high temperatures or low humidities. For example, some PEMs with domain sizes < 5 nm in the dry state exhibited increases in conductivity with increasing temperature up to 90 °C. They proposed that the suppression of water evaporation from the PEMs was due to the capillary condensation of the water in confined nanochannels, thus reducing its chemical potential. From these studies we can conclude that the morphology in self-assembled PEMs and the size of the ionic phase are critically important to achieve a material with high proton conductivity at high temperatures and low humidities.

We aim to produce new cross-linked PEMs that (i) adopt a bicontinuous structure, (ii) contain a SPS phase, (iii) possess tunable domain sizes, and (iv) are mechanically and thermally robust. To this end, we prepared a series of poly(norbornenylethylstyrene−styrene)−poly(*n*-propyl-*p*-styrenesulfonate) (PNS−PSSP) block copolymers by atom transfer radical polymerization (ATRP) and utilized these materials in a polymerization-induced phase separation scheme to yield robust precursor membranes (Figure 1).[28,54] These materials were converted into PEMs with bicontinuous structures where the size of the ionic domains is controlled by the molecular weight of the PNS−PSSP copolymer. The proton conductivities of some of these PEMs were similar to Nafion at high humidity, and membrane swelling was managed by tuning the modulus of the structural phase. The PEM that exhibited the least amount of swelling gave the lowest methanol permeability while still retaining high-saturated proton conductivity. These membranes hold a great deal of promise as PEMs for highly efficient DMFCs.

Results and Discussion

Polymer Synthesis and Characterization. Ionic block copolymers containing poly(styrenesulfonic acid) are typically produced by sulfonation of a PS-containing block[19−27] or by radical polymerization of sodium styrenesulfonate.[17,18] In these examples, the processabilities of the resultant copolymers can be compromised by their ionic character. The polymerization of styrenesulfonate esters, on the other hand, allows for the synthesis of copolymers with tailored levels of sulfonation using controlled free radical polymerization followed by base hydrolysis.[29,30] The approach shown schematically in Figure 1 requires the synthesis of a reactive block polymer containing a norbornene-functional PS block for ultimate metathesis cross-linking as in our previous work[28] and a polystyrenesulfonate ester block as the precursor to a proton conducting phase. To this end, *n*-propyl-*p*-styrenesulfonate (SSP) was synthesized by the esterification of styrenesulfonyl chloride and *n*-propyl alcohol, and norbornenylethylstyrene (N) was prepared by our previously reported method.[31]

Atom transfer radical polymerization (ATRP) has been utilized for the controlled polymerization of a variety of styrene derivatives including styrenesulfonate esters.[32] We prepared poly(norbornenylethylstyrene-*s*-styrene)−poly(propyl-*p*-styrenesulfonate) (PNS−PSSP) block polymers by sequential ATRP reactions (Scheme 1). The PNS block was prepared by ATR copolymerization of N and styrene, using 1-bromoethylstyrene as the initiator. By manipulating the relative amounts of the comonomers and the initiator, we were able to prepare bromo-terminated PNS samples with tailored molecular weights and norbornene contents as summarized in Table 1. SEC analyses of these polymers gave polydispersity indices (PDIs) around 1.5, consistent with styrene homopolymerizations under similar conditions.[33] The M_n and N content of PNS blocks were determined by NMR spectroscopy (Table 1). Between 4 and 12 norbornene groups were incorporated into the PNS blocks.[34]

ATRP of SSP using the bromo-terminated PNS as a macroinitiator resulted in near-quantitative conversion of SSP and the formation of PNS−PSSP block polymers in 60−80% isolated yield. The less than quantitative yields were attributed to mass losses that occurred during removal of the Cu catalyst (see Experimental Section). The M_n of the PSSP was determined using ^{1}H NMR spectroscopy and the predetermined M_n of the PNS block. A representative ^{1}H NMR spectrum for PNS−PSSP (2−5) is shown in Figure S2; the retention of both norbornene and sulfonate ester functional groups is evident. The SEC data for PNS−PSSP (2−5) is shown in Figure S1; a clear shift to lower elution volume for this sample compared to PNS (2) confirms the conversion of the bromo-terminated PNS to the PNS−PSSP block polymer. However, SEC analysis of the two higher molecular weight PNS−PSSP samples in $CHCl_3$ using either a differential refractive index detector or a UV−vis detector produced very weak signals. This may be due to interactions between the sulfonate ester block and the column packing material. The PNS−PSSP (6−13) and PNS−PSSP (10−23) copolymers were evaluated by SEC in THF containing 1 vol % *N*,*N*,*N*′,*N*′-tetramethylethylenediamine and using a combination of refractive index and light scattering detectors. While a peak associated with the copolymer was observed, a high molecular weight tail was evident in both samples. We attribute this high molecular weight signal to aggregation of

Table 1. Molecular Characteristics of PNS Macroinitiators and PNS−PSSP Block Polymers

entry[a]	NMR M_n (kg mol^{-1})	SEC M_n (kg mol^{-1})[b]	PDI	PSSP (wt %)	av no. of N per chain	mol % N in PNS[d]	D (nm)[e]
PNS (10)	10.1	9.2	1.55		12	0.14	
PNS−PSSP (10−23)	33.0	20.9[c]		70	12	0.14	24
PNS (6)	5.9	6.4	1.45		7	0.14	
PNS−PSSP (6−13)	18.9	14.4[c]		69	7	0.14	15
PNS (2)	2.0	2.5	1.23		4	0.32	
PNS−PSSP (2−5)	6.5	4.2	1.19	69	4	0.32	10

[a] PNS (A) and PNS−PSSP (A−B) denote a bromo-terminated PNS and a PNS−PSSP copolymer, where A and B indicate the NMR M_n values (in kg/mol) for the PNS and PSSP blocks, respectively. [b] SEC data acquired in $CHCl_3$ using a RI detector and PS standards. [c] Peak M_n values obtained by SEC in THF using a combination of refractive index and light scattering detectors based on PS. [d] x in Scheme 1. [e] Domain spacing (D) in copolymers was obtained through SAXS analysis at 100 °C and calculated based on $D = 2\pi/q^*$, where the q^* is the primary peak position in the 1D SAXS plot.

Scheme 1. Synthetic Protocol for PNS−PSSP Block Polymers

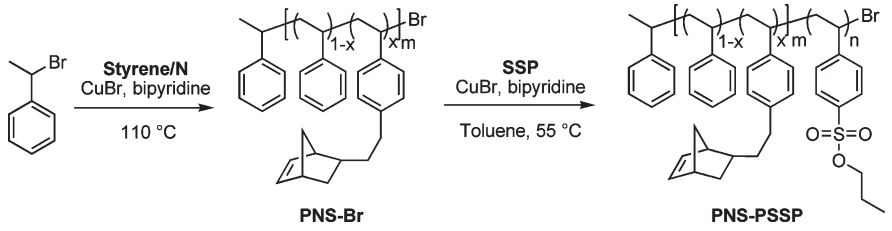

Table 2. Summary of the Cross-Linked Precursor Films

entry[a]	PNS−PSSP sample	monomer(s)	PNS−PSSP (wt %)	PSSP[b] (wt %)	D[c] (nm)	f_a[c]
PEM1e	PNS−PSSP (10−23)	COE	59.9	41.6	37.3	−0.48
PEM2e	PNS−PSSP (6−13)	COE	64.1	44.1	17.7	−0.87
PEM3e	PNS−PSSP (2−5)	COE	59.9	41.5	10.5	−0.86
PEM4e	PNS−PSSP (6−13)	COE:DCPD (1:1)	60.6	41.7	27.3	−0.72
PEM5e	PNS−PSSP (6−13)	DCPD	61.3	42.2	19.0	−0.71

[a] "e" indicates these precursor membranes contain the sulfonyl group in the ester form. [b] PSSP content in the cross-linked precursor films, given all components were fully cross-linked. [c] Domain spacing (D) and amphiphilicity factor (f_a) determined by SAXS analysis using the Teubner−Strey model.[37]

the PNS−PSSP block polymers in THF based on preliminary dynamic light scattering analysis of a dilute solution of PNS−PSSP (10−23). The peak molecular weights of these copolymers from this analysis based on PS standards are given in Table 1.

DSC analysis of these copolymers (between −40 and 200 °C) only revealed one T_g associated with the PNS block (between 90 and 100 °C). The morphologies of these copolymers were probed by small-angle X-ray scattering (SAXS). Each of the copolymer samples exhibited a principal scattering peak indicative of microphase separation between the PNS and PSSP blocks. The domain spacing increased with increasing PNS−PSSP molecular weight as expected. However, due to lack of high-order reflections, even after annealing these copolymers at 150 °C for 10 min, no specific morphology could be determined. Possibly, equilibration in these copolymers was hindered by the high glass transition temperature (T_g) of the PSSP block, which has been reported to be higher than 200 °C.[35] Heating the PNS−PSSP block polymers to temperatures higher than 200 °C resulted in an irreversible exothermic transition as determined by DSC. Consistent with this observation, in SAXS experiments performed at 195 °C for 10 min, an irreversible change of domain spacing (Figure S3) indicated decomposition of the PSSP block before achieving an equilibrium morphology. It was further confirmed by IR spectroscopy that the PSSP block was converted into poly(styrenesulfonic acid) (PSSA) after prolonged annealing (Figure S4); thermal decomposition of similar PS sulfonate esters has been previously reported.[29]

Cross-Linked Precursor Membranes. In our previously reported nanoporous membrane synthesis, a PNS−polylactide (PLA) block polymer containing a metathesis reactive segment (PNS) and a chemically etchable segment (PLA) was combined with dicyclopentadiene (DCPD) and a ruthenium-based metathesis catalyst in a suitable solvent to give robust nanostructured membranes upon casting, curing, and drying. Removal of the PLA component from these membranes yielded nanoporous samples with bicontinuous morphologies.[28]

Here we take a similar approach using PNS−PSSP as the doubly reactive block polymer and DCPD and/or cyclooctene (COE) as the metathesis reactive comonomers to produce nanophase-separated bicontinuous morphologies (Figure 1). PNS−PSSP samples and reactive monomers were dissolved in THF to give an optically homogeneous solution. The second-generation Grubbs metathesis catalyst[36] dissolved in a minimum amount of THF was added to the solution of PNS−PSSP and monomers. Cast films formed gels in about 2 min and were allowed to cure at room temperature (RT) overnight and then at 90 °C for 1 h. For this study, we prepared five cross-linked precursor films containing roughly 42 wt % PSSP (Table 2). The resultant films were transparent and slightly yellow. The color was due to the low levels of metathesis catalyst that remained in the films.

Table 2 summarizes the properties of the cross-linked precursor, PEMXe, films, where "e" indicates that the films contain sulfonate groups in the ester form. Transmission electron microscopy (TEM) analysis demonstrated that similar structures were adopted in all samples. As an example, a TEM micrograph of a cryo-microtomed slice of PEM2e is shown in Figure 2. In this image, the bright domains correspond to the unstained PSSP phase, and the

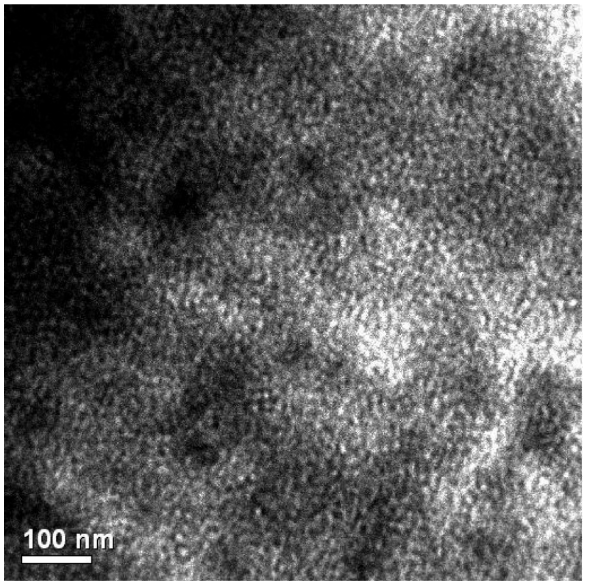

Figure 2. TEM micrograph of PEM2e. The film was cryo-microtomed and stained with OsO_4; the PCOE-containing PNS domains appear dark.

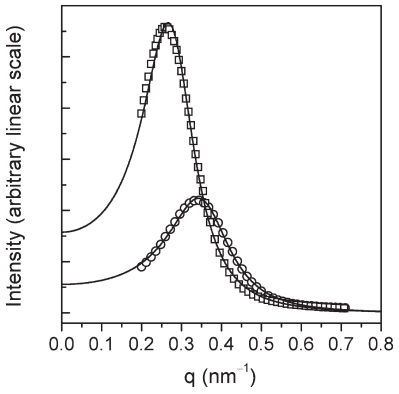

Figure 3. Synchrotron X-ray scattering profiles of the PEM2e (circles) and the PEM2a (the "a" indicates the acid form of the membrane) (squares) with curve fitting using the Teubner−Strey model.[37] The difference in scattered intensity is due to the increased scattering contrast for the acid form of the membrane.

dark domains are the PCOE-containing phase with the backbone double bonds selectively stained by OsO_4. A microphase-separated morphology with interconnected PSSP domains (ca. 18 nm in width) is evident from this image.

Synchrotron SAXS experiments were conducted to probe the microstructure in the resultant PEMXe samples. A single scattering peak was observed for each of the membranes and suggested a phase-separated but disorganized structure. We analyzed the scattering data using the Teubner−Strey model[37] for a bicontinuous microemulsion given the structural similarities indicated by the TEM image (Figure 2). The scattering profile and Teubner−Strey fit for PEM2e are shown in Figure 3 (SAXS profiles and fits for the other PEMXe membranes are given in Figure S7). A domain spacing (d) and amphiphilicity factor (f_a) were extracted using this model.[37] The amphiphilicity factor is a parameter that describes the character of bicontinuous microemulsions. For example, a value of f_a between −1 and 0 indicates a well-defined bicontinuous phase.[38] The values of f_a for the PEMXe membranes (Table 2) were between −0.86 and −0.48.

Table 3. Summary of Tensile Tests on the Precursor Films

entry	Young's modulus (MPa)	tensile strength (MPa)	elongation at break (%)
PEM1e	315 ± 11	21.6 ± 1.3	176 ± 16
PEM2e	422 ± 42	22.4 ± 1.0	152 ± 3
PEM3e	416 ± 42	19.5 ± 1.0	70 ± 11
PEM4e	520 ± 20	27.8 ± 1.9	126 ± 13
PEM5e	993 ± 49	30.0 ± 2.5	13 ± 3

The domain spacing of PEM2e by SAXS (17.7 nm) was consistent with TEM data (Figure 2). Furthermore, the domain spacings of PEMs 1e, 2e, and 3e decreased with decreasing molecular weight of PNS−PSSP. The domain spacings of PEMs 4e and 5e were both larger than that of PEM2e produced using the same molecular weight copolymer but different cross-linking monomer. The difference could be partially accounted for by the higher fraction of monomer in PEMs 4e and 5e and the difference in the nature of the cross-linked matrix phase (see below). From the above results, we hypothesize that during the *in situ* metathesis reactions of PNS−PSSP and the reactive monomers the PNS component and the monomers were polymerized to render a highly interconnected structure, favoring a bicontinuous phase based on the example of *in situ* grafting polymerization in a binary polymer blend.[39]

The tensile properties of the dry PEMXe membranes were examined under ambient conditions (Figure S5) and are summarized in Table 3. The modulus, tensile strength, and elongation at break values for the PEM1e−4e samples were comparable to the parent PCOE homopolymer: moduli between 300 and 540 MPa, tensile strengths between 20 and 28 MPa, and elongations at break between 70% and 190% were observed. In the dry state, Nafion has a modulus of about 250 MPa, a tensile strength of about 35 MPa, and an elongation at break of about 250%.[40] PEM5e exhibited a higher modulus and tensile strength but lower elongation at break due the higher level of DCPD in the monomer mixture.

PEM Synthesis. The PSSP block in these precursor films was hydrolyzed by treatment with a concentrated NaOH solution. Protonation of the sulfonate groups was accomplished using aqueous HCl (see Experimental Section for details). IR characterization confirmed that the PSSP component in all precursor films was fully converted into the acid form. The IR spectra of PEM2e and PEM2a (the "a" indicates the acid form of the membrane) are shown in Figure S6. The PEM2e membrane exhibited strong absorbance at 1370 and 1170 cm^{-1} for the SO_2 stretching of sulfonate ester; upon hydrolysis, these absorbance bands were absent, and a characteristic band for the SO_3^- stretching of sodium sulfonate group was observed at 1200 cm^{-1}; after protonation, an absorbance band associated with the sulfonic acid group at 1155 cm^{-1} was observed.

Synchrotron SAXS analysis of the resulting acid PEMXa dried samples at ambient conditions displayed a single scattering peak that was well fit by the Teubner−Strey model as in the PEMXe samples.[37] Representative SAXS data for PEM2a are given in Figure 3 (see Figure S7 for SAXS data on the other PEMXa membranes). The increased scattering intensity for PEM2a as compared to PEM2e is likely due to the enhanced electron density difference between the acid phase and the matrix phase.

A summary of the SAXS results (D and f_a values) for the PEMXa membranes is given in Table 4. Interestingly, the domain spacings of the PEMXa membranes containing only PCOE were consistently larger than their corresponding PEMXe precursors. This phenomenon is likely due to the increase in the Flory−Huggins parameter between PSSA

Table 4. Summary of the Resultant PEMs

				PSSA width (nm)		IEC (mmol/g)	
entry[a]	PSSA[b] (wt %)	D[c] (nm)	f_a	SAXS[d]	TEM[e]	predicted[f]	measured[g]
PEM1a	36.7	41.5	−0.50	18.7	19	2.00	1.98
PEM2a	39.1	22.6	−0.85	10.8	11	2.12	2.06
PEM3a	36.6	14.4	−0.86	6.6	7	1.99	1.93
PEM4a	36.8	28.3	−0.68	13.0	10	2.00	1.86
PEM5a	37.3	19.5	−0.71	9.0	8	2.03	1.96

[a] "a" indicates these membranes contain sulfonyl group in acid form. [b] Composition of the PSSA phase in each PEM was calculated based on the membrane composition based on the PSSP composition. [c] Domain spacing (D) was calculated from SAXS analysis. [d] Estimated PSSA domain size from SAXS analysis described in the Supporting Information. [e] Estimated PSSA domain size from TEM micrographs, ±1 nm. [f] Moles of sulfonic acid per gram of sample, calculated based on the PSSA content: IEC = 1 (g) × (PSSA wt %)/184 (g/mol) × 1000/1 (g), in units of mmol/g. [g] Determined by elemental analysis.

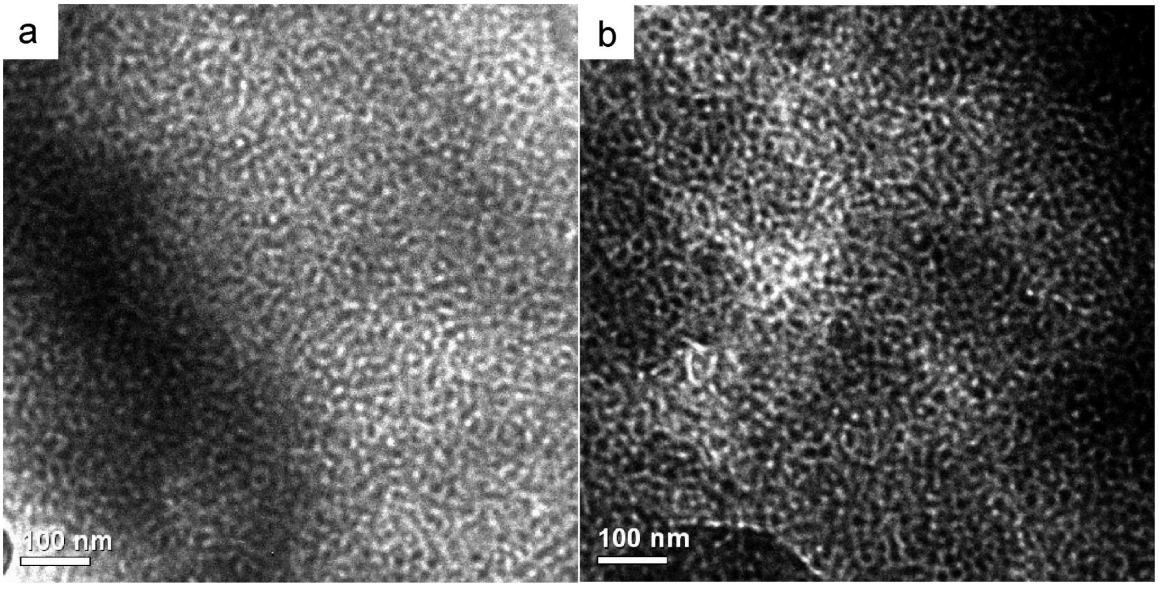

Figure 4. TEM images of PEM2a: (a) the film was cyro-microtomed and stained by OsO_4; (b) the film was stained in a saturated $Pb(acetate)_2$ aqueous solution and then cyro-microtomed.

and the matrix; the relatively soft and ductile PCOE domains could accommodate domain increases. Consistent with this, the PDCPD containing membranes PEM4a and PEM5a exhibited domain spacings that were approximately the same as the PEM4e and PEM5e samples. We estimated the sizes of the individual PSSA domains using simple cylindrical and lamellar models, and the averages are given in Table 4 (see Supporting Information for details). Ion exchange capacity (IEC) in these PEMs was calculated based on the predicted PSSA content and determined by elemental analysis (EA). In general, these measured IEC values were in good agreement with the anticipated values. The somewhat lower IEC values from EA may be attributed to absorbed moisture in these PEMXa films under ambient conditions. An absorbance associated with water in the IR spectra (3400 cm^{-1}) in the PEMXa films is consistent with this notion.

From the Teubner−Strey analysis, amphiphilicity factors between −0.86 and −0.50 were extracted for the PEMXa membranes. Supporting evidence for the bicontinuous structure was provided by TEM analysis. A TEM image of thin section of PEM2a with OsO_4 staining is given in Figure 4a; the bright domains correspond to the PSSA. TEM analysis of all PEMXa membranes was also performed using a Pb^{2+} stain.[18] This reverses the contrast from the OsO_4. The TEM image for PEM2a shown in Figure 4b is similar in structure and domain spacing to that in Figure 4a. TEM images for other PEMXa membranes are shown in Figure 5. The PSSA domain sizes in the resultant PEMXa membranes were estimated from these TEM images. For PEMs 1a, 2a, and 3a, the PSSA domain size increases with the length of the PSSA block, and the PSSA domain sizes measured from TEM images were comparable with those values estimated by SAXS analyses. PEMs 2a, 4a, and 5a all contain the same molecular weight precursor, PNS−PSSP (6−13). A consistent decrease in the PSSA size was observed with increasing DCPD content in the matrix phase in these PEMs.

DSC analysis of PEMs 1a, 2a, and 3a (Figure S8) showed melting endotherms between 0 and 50 °C upon heating consistent with the semicrystalline nature of PCOE. Decreased melting temperature (T_m) and crystallinity of PCOE generally agreed with the reduced domain sizes. No thermal transitions were observed for PEMs 4a and 5a up to 120 °C (Figure S8). SAXS analysis of PEMXa indicated persistent scattering peaks at high temperatures (150 °C), for example, the SAXS profiles for PEM 2a shown in Figure S9. In contrast, morphologies of un-cross-linked PEMs from block copolymers were sensitive to both humidity and temperature.[41] Tensile testing of PEM2a (Figure S10) under ambient conditions indicated an elongation at break of 90% and a tensile strength of 21 MPa.

Methanol Permeability and Proton Conductivity Measurements. Prior to testing the PEMXa membranes any surface skin layer was completely removed using O_2 plasma etching.[28] As a confirmation of effective skin removal, XPS analysis (Figure S11) of the surface of PEM1a after etching indicates a sulfur composition (5.8 wt %) comparable to that in bulk (6.4 wt %).

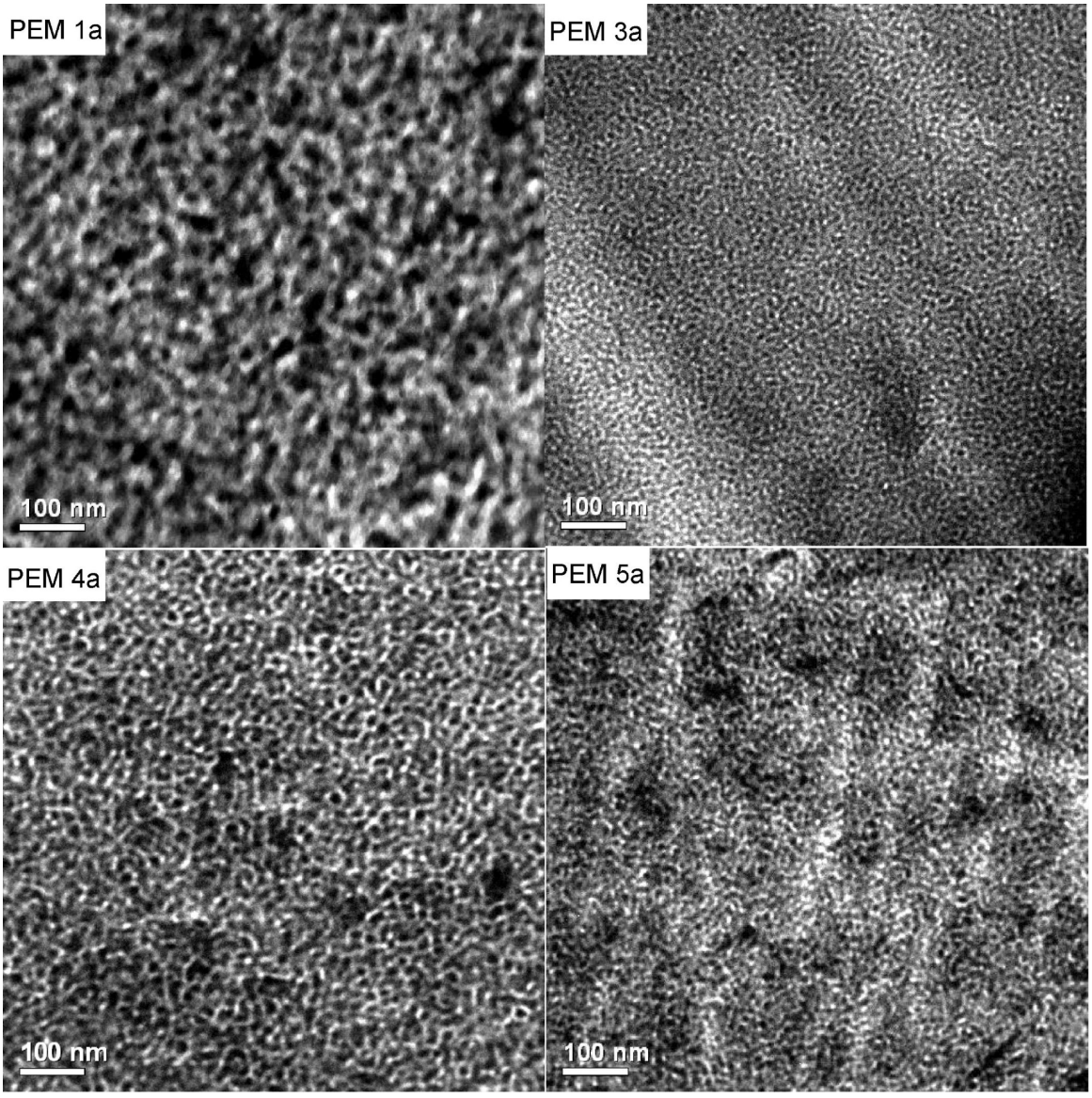

Figure 5. TEM images of four PEMXa membranes. The membranes were cryo-microtomed and stained by $Pb(acetate)_2$, and dark domains correspond to the $PSSA/Pb^{2+}$ phase.

Table 5. Water Sorption and Swelling for the PEMXa Membranes

		swelling					
sample	dry thickness (μm)	thickness (%)	width (%)	length (%)	volume (%)	water uptake (%)	λ (mol H_2O/mol SO_3H)
PEM1a	335 ± 32	30 ± 4	26 ± 0.4	28 ± 1	108 ± 6	118 ± 4	33 ± 1
PEM2a	243 ± 44	21 ± 5	20 ± 3	19 ± 1	68 ± 7	73 ± 12	21 ± 4
PEM3a	195 ± 16	21 ± 2	21 ± 5	18 ± 6	77 ± 1	78 ± 5	22 ± 1
PEM4a	184 ± 28	26 ± 3	19 ± 1	19 ± 0.1	78 ± 3	73 ± 2	20 ± 0.4
PEM5a	233 ± 21	21 ± 2	11 ± 1	11 ± 1	48 ± 0.3	42 ± 0.4	12 ± 0.1
Nafion 117	180 ± 2	20 ± 2	16 ± 2	19 ± 1	65 ± 2	34 ± 0.4	21 ± 0.2

Table 5 lists the water sorption and swelling properties of each PEMa. Consistent with the isotropic morphology indicated by the SAXS and TEM analysis, isotropic swelling was observed for PEM1a, 2a, 3a, and 4a. Some swelling anisotropy was observed for PEM5a. PEMs 2a, 3a, and 4a all have similar swelling and normalized water uptake λ (mol H_2O/mol SO_3H) behavior as Nafion. Interestingly, PEMs with such high IEC values (double that of Nafion) typically result in much higher λ values than we observed for the PEMXa membranes (typically, $\lambda \approx 100$ at IEC $\approx$ 2 mmol/g).[42] The cross-linked nature of the PEMXa membranes is likely responsible for this behavior. For DMFC applications, low volumetric swelling is desirable for long-term operational stability; thus, PEM5a with DCPD cross-linker as the sole monomer is optimal.

All PEMXa samples had similar conductivities compared to Nafion (ca. $(1-3) \times 10^{-2}$ S/cm). Interestingly, proton conductivity in PEMXa samples were independent of water content, contrary to typical sulfonated polymers where conductivity has been shown to be strongly dependent on water content (see Figure S12).[24c,43,44] For example, sulfonated triblock copolymers at similar λ to Nafion resulted in

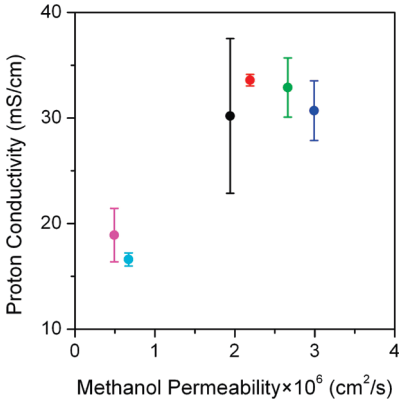

Figure 6. Two-electrode (through-plane) proton conductivity and methanol permeabilities of PEM1a (red), PEM2a (green), PEM3a (blue), PEM4a (cyan), PEM5a (magenta), and Nafion (black).

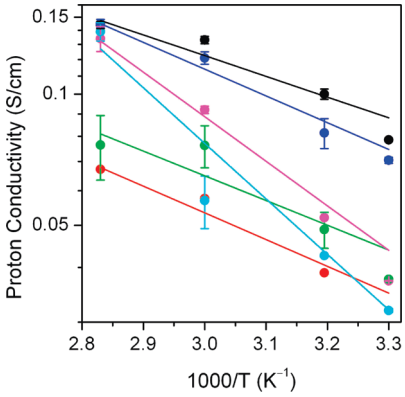

Figure 7. Four-electrode (in-plane) proton conductivity versus temperature at 90% RH for Nafion (black), PEM1a (red), PEM2a (green), PEM3a (blue), PEM4a (cyan), and PEM5a (magenta).

conductivities an order of magnitude lower than Nafion. Furthermore, increasing λ in the sulfonated triblock polymers to values similar to PEM5a resulted in even lower conductivities.[24c]

Figure 6 shows measured methanol permeabilities as a function of through-plane proton conductivity. In most studies on sulfonic acid containing polymers, methanol permeability and proton conductivity typically increase or decrease in unison.[8g] Surprisingly, the methanol permeability for PEM5a was 4-fold lower than Nafion 117 at a similar proton conductivity. Furthermore, methanol permeability decreases with increasing domain size; PEM1a has a lower permeability compared to PEM2a and 3a. PEM4a and 5a (both with DCPD cross-linker) have significantly lower methanol permeabilities than Nafion at only slightly reduced proton conductivities.

Methanol permeability is a product of two key properties: methanol sorption and methanol diffusivity. In a recent report by Hallinan and Elabd[45] time-resolved FTIR-ATR spectroscopy was used to measure multicomponent sorption and diffusion of methanol and water in Nafion. The authors concluded that the main contributing factor to the increase in methanol permeability (or flux) with increasing methanol solution concentration was methanol sorption and not methanol diffusion. We suggest that the incorporation of DCPD leads to increased cross-linked density, thereby lowering methanol flux while maintaining high proton conductivity. However, the precise mechanism that results in high proton conductivity and low methanol permeability in PEMXa membranes is still unclear. At comparable proton conductivity, the selectivity (proton conductivity (in mS/cm)/methanol permeability (in 10^{-6} cm^2/s)) is greater than 30 for PEM5a whereas Nafion is ca. 15. This differs from many studies, where similar selectivities have been observed in most sulfonic acid containing polymers regardless of ion content, water content, polymer chemistry, architecture, or morphology.[8g] Polymer membranes with conductivities similar to Nafion and higher selectivities are highly desirable for improved DMFC performance, and PEM4a and PEM5a are among the best performing membranes that were recently reviewed.[8g]

Figure 7 shows the in-plane (four-electrode) proton conductivity for all samples as a function of temperature at a fixed relative humidity (RH) of 90%. At a given temperature, the differences in proton conductivity between the PEMXa samples are slightly more significant than the through-plane conductivities. This may be attributed to the different environment (water vapor), which would result in different water contents in each sample compared to the liquid water saturated conditions used in the through-plane conductivity measurements. The effect of domain size can be seen by comparison of PEM1a (red), PEM2a (green), and PEM3a (blue). Conductivity increases at all temperatures with decreasing domain size, and PEM3a with the smallest domain size exhibited the highest conductivity. In fact, the PEM3a was nearly identical to Nafion at all temperatures. This conductivity dependence on domain size is consistent with the work of Park et al. in ref 27 and could be the result of capillary condensation effects in the smaller domain size materials. PEM1a, PEM2a, and PEM3a all show a similar temperature dependence on conductivity compared to Nafion at 90% RH.

Table 6. Activation Energies

sample	E_A (90% RH)[a] (kJ mol^{-1})	E_A (50% RH)[a] (kJ mol^{-1})
PEM1a	12 ± 5	10 ± 1
PEM2a	13 ± 2	18 ± 2
PEM3a	14 ± 3	24 ± 21
PEM4a	25	17
PEM5a	23	31
Nafion 117	10 ± 2	24 ± 4

[a] Values correspond to average and standard deviation determined from analyzing more than one experiment with the exception of PEM4a and PEM5a.

PEM2a (green), PEM4a (cyan), and PEM5a (magenta) have similar domain spacings and similar conductivities at low temperatures (30 and 40 °C)—approximately half of the conductivity of Nafion. However, at higher temperature (80 °C), the conductivities of PEM4a and PEM5a both of which incorporate DCPD as a cross-linking monomer are similar to that of Nafion. To this end, Table 6 shows that PEM1a, PEM2a, and PEM3a have approximately the same activation energy as Nafion at 90% RH (10 ± 2 kJ/mol),[24a,24c,46,47] while PEM4a and PEM5a have nearly a 2-fold higher activation energy for proton conductivity. This suggests that at high humidity the DCPD cross-linker has a significantly different effect than the COE cross-linker on proton conductivity at higher temperatures.

Figure 8 shows the in-plane (four-electrode) proton conductivity for all samples as a function of temperature at a lower fixed relative humidity of 50% RH. Similar to 90% RH data, PEM1a (largest domain spacing) is lower in conductivity compared to PEM2a and both are lower in conductivity compared to Nafion. Also, listed in Table 6, the activation energy for PEM1a remains relatively unchanged

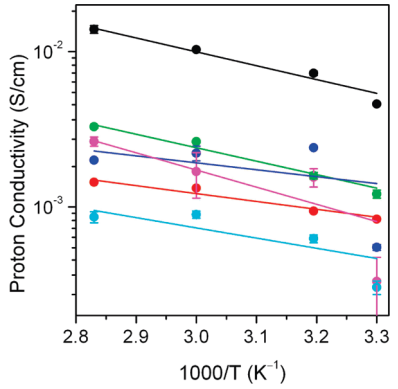

Figure 8. Four-electrode (in-plane) proton conductivity versus temperature at 50% RH for Nafion (black), PEM1a (red), PEM2a (green), PEM3a (blue), PEM4a (cyan), and PEM5a (magenta).

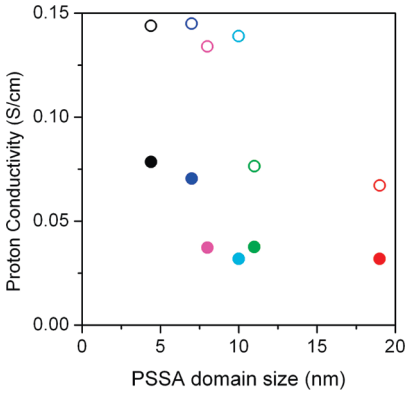

Figure 9. Four-electrode (in-plane) proton conductivity versus domain size at 90% RH for Nafion (black), PEM1a (red), PEM2a (green), PEM3a (blue), PEM4a (cyan), and PEM5a (magenta), where open and filled symbols correspond to 80 and 30 °C, respectively. The domain size for Nafion in this figure corresponds to the ionic domain size determined by TEM measurements in ref 55.

compared to the 90% RH data, while the activation energies for PEM2a and Nafion are similar and both increase to ~20 kJ/mol compared to 90% RH. Contrary to the 90% RH data, PEM3a has a lower conductivity when compared to Nafion and appears to have an irregular temperature dependence with a poor fit to an Arrhenius model. At 50% RH, PEM2a (green), PEM4a (cyan), and PEM5a (magneta) all have conductivities lower than Nafion at all temperatures. Unlike the 90% RH data, the conductivities of PEM4a and PEM5a at 50% RH do not have conductivities similar to Nafion at higher temperatures. Similar to PEM3a, the PEM4a and 5a samples also have an irregular dependence on temperature. Interestingly, PEMs 3a, 4a, and 5a all have the smallest ionic domain size (Table 4). The data presented in Figures 7 and 8 suggest that PEMXa samples have different proton conductivity−water content relationships when compared to other sulfonated polymers.[8g] This may be attributed to cross-linking resulting in different (and reduced) water contents at given IECs.

Figure 9 shows the in-plane conductivity at 90% RH at both 30 and 80 °C for all samples as a function of the ionic domain size (Table 4). Caution should be taken when interpreting these results as the domain sizes were measured for dry samples and conductivity values were measured on samples equilibrated under humid conditions. However, it is interesting to note that at both temperatures proton conductivity appears to increase with decreasing ionic domain size. Similar results have been observed in the literature for nanopore-filled membranes, where the pores were filled with cross-linked grafted polyelectrolytes and proton conductivities in these membranes increased significantly with decreasing pore size (particularly as the pores approached 10 nm).[48] Balsara and co-workers[27] have also observed increased conductivities in sulfonated block copolymers with ionic domain sizes less than 5 nm.

Conclusions

We have demonstrated a facile method for the preparation of cross-linked PEMs from PNS−PSSP block polymers and reactive cyclic olefins. A bicontinuous morphology with continuous PSSA domains supported by a continuous and mechanically robust phase was evident in these films. Pronounced thermal and mechanical stabilities in the resultant PEMs was realized. PSSA domain size was tuned by the copolymer molecular weight. Select PEMs showed much lower methanol crossover than Nafion while maintaining high-saturated proton conductivities. This is a significant result, since many previous studies have found that the trends in methanol crossover and proton conductivity are coupled in PEMs. This reactive block polymer strategy for the preparation of PEMs is attractive due the ready formation of bicontinuous structures, the facile control of domain size, and the ability to independently control mechanical and swelling properties of the matrix material. Potentially, the novel preparation allows for facile increase in the acid content in PEMs having small PSSA domain size while maintaining the membrane robustness. We anticipate enhanced DMFC performance using these membranes given that recently reported blend membranes with similarly low methanol permeability and high conductivity out perform Nafion in terms of maximum power density at high methanol concentrations.[49]

Experimental Section

Materials. Styrene (≥99%) and *cis*-cyclooctene (COE) (95%) were purchased from Aldrich, purified by passage through short columns packed with active alumina (to remove the radical inhibitors), and distilled over CaH_2 under reduced pressure. Norbornenylethylstyrene (N) was prepared according to the procedure described elsewhere.[31] *p*-Propyl-*n*-styrenesulfonate (SSP) was synthesized using a reported procedure. [29] Toluene (≥99.9%) was degassed by purging with nitrogen and rigorously purified by passage through a home-built solvent purification system equipped with activated alumina and a supported copper catalyst to remove traces of protic impurities.[50] Copper(I) bromide (≥98%), thionyl chloride (≥99.0%), and sodium 4-styrenesulfonate (≥90%) were obtained from Fluka and used without purification. Pyridine (≥99.0%) and *N,N*-dimethylformamide (DMF) (≥99.9%) were distilled over CaH_2 under reduced pressure. 2,2′-Bipyridine (≥99%), *n*-propanol (99.7%), 1-bromoethylstyrene (97%), and dicyclopentadiene (DCPD) were obtained from Aldrich and used as received. Nafion 117 (1100 EW, 178 μm, commercially extruded film) was purchased from Aldrich. 1100 EW corresponds to an ion exchange capacity (IEC) of 0.91 mmol of sulfonic acid per gram of polymer. The following chemicals were used to purify Nafion membranes: hydrogen peroxide (30−32 wt %) diluted to 3 wt %, ultrapure deionized (DI) water (resistivity ~16 MΩ cm), and sulfuric acid (99.999%). Methanol (Aldrich, ≥99.8%) was used in permeability experiments.

General Methods. All NMR spectra were acquired on a Varian 300 VI spectrometer at RT, and samples were dissolved in $CDCl_3$ (Cambridge) at a concentration of about 1 wt %. Size exclusion chromatography (SEC) analyses were mostly performed in $CHCl_3$ (1 mL/min) at 35 °C using a Hewlett-Packard 1100 series liquid chromatograph equipped with three PLgel 5 μm mixed columns and a Hewlett-Packard 1047A refractive index detector. The SEC instrument was calibrated with

polystyrene standards (Polymer Laboratories). Some SEC data were collected using a system consisting of a Wyatt Optilab RI detector, a Wyatt Dawn multiangle light scattering detector, and three Phenolgel columns of 10^5, 10^4, and 10^3 Å pore sizes, where THF with 1 vol % *N,N,N′,N′*-tetramethylethylenediamine was used as the mobile phase at 40 °C with a flow rate of 1 mL/min, and molecular weights were extracted based on PS standards. Differential scanning calorimetry (DSC) experiments were conducted on a TA Instruments Q1000 at a heating rate of 10 °C min^{-1}. Fourier transform infrared (FT-IR) spectra were collected on a Nicolet Magna-Infrared spectrometer 550. Transmission electron microscopy (TEM) micrographs were obtained on a JEOL 1210 transmission electron microscope at 120 kV accelerating voltage. Some polymer samples were cryo-microtomed at −120 °C into about 80 nm thick slices and then stained with 4 wt % OsO_4 aqueous solution for 15 min; other samples were first soaked in a saturated aqueous solution of $Pb(acetate)_2$ overnight and subseqently cryo-microtomed into about 80 nm thick slices at −120 °C. Tensile tests were conducted under ambient conditions using a Rheometric Scientific MINIMAT instrument with a 200 N load cell installed at crosshead speed of 4 mm/min. Measured films were cut into rectangular bars (3.0 × 0.5 × 0.1 cm). Some small-angle X-ray scattering (SAXS) experiments were performed on a 3.7 m custom-built beamline at the University of Minnesota. Cu Kα X-rays (λ = 1.542 Å) were generated through the use of a rotating anode. Samples were equilibrated under vacuum for 300 s before collection. The 2-D images were azimuthally integrated to a 1-D plot of intensity vs q where $q = 4\pi/\lambda \sin(\theta/2)$ and θ and λ are the scattering angle and X-ray wavelength, respectively. Other SAXS data for curve fitting were acquired at the Argonne National Lab using the synchrotron source at Sector 5-ID-D beamline. The source produces X-rays with a wavelength of 0.84 Å. The sample-to-detector distance was 5.65 m, and the detector radius is 81 mm. Scattering intensity was monitored by a Mar 165 mm diameter CCD detector. The 2-D scattering patterns were azimuthally integrated to generate 1-D plot of scattering intensity vs q.

Synthesis of Norbornene-Functional Polystyrene. PNS macroinitiators were prepared by atom transfer radical polymerizations following the reported procedure.[33] 1-Bromoethylstyrene, CuBr, and bipyridine in a molar ratio of 1:1:2 were mixed with styrene and monomer N (the monomer ratio variable) in bulk or 20% in toluene in an air free flask under an argon atmosphere, followed by three freeze−pump−thaw cycles. The reaction vessels were sealed under vacuum and placed in an oil bath at 110 °C. For PNS(10) and PNS(6), the mole ratio of monomers to the initiator was 162, and the bulk polymerizations proceeded for 6 and 4 h, respectively; for PNS(2), the mole ratio of monomers to the initiator was 28, and the reaction time was 4 h in a 20% toluene solution. After polymerizations, the reaction mixtures were diluted with THF and passed through short alumina columns to remove the residue catalysts. The resultant polymers were recovered through precipitation in methanol followed by vacuum filtration, washed with extra methanol, and finally dried at 60 °C overnight under reduced pressure. Overall monomer conversions were between 40 and 60 wt %. ^{1}H NMR spectroscopy was employed to determine the number-average molecular weight (M_n) by end-group analysis and compositions in resultant polymers. ^{1}H NMR spectrum of PNS (300 MHz, $CDCl_3$) (multiplicity, identity) δ ppm: 6.2−7.3 (b, Ar*H*), 5.9−6.2 (b, −C*H*=C*H*−), 4.3−4.6 (b, −C*H*−Br), 2.8 (b, −C*H*−CH=CH−C*H*−), 2.5 (b, Ar−CH_2−), 0.6−2.0 (b, remaining C*H* and CH_2).

Synthesis of the PNS−PSSP Copolymers.[29] PNS−PSSP copolymers were synthesized via an ATRP scheme using the bromo-terminated PNS. PNSBr (0.4 g), SSP (0.8−1.0 g), CuBr, and bipyridine were dissolved in dry toluene (1 mL), where the molar ratio of PNSBr, bipyridine, and CuBr was 1:2:4. After three freeze−pump−thaw cycles, the reaction solutions were kept under vacuum and reacted at 55 °C for 20 h. The resulting brown mixtures were diluted with excess acetone, and the catalyst was removed by passage through short columns filled with Dowex ion exchange resins (sodium form) several times until the solutions were light-colored. The resultant copolymers were recovered by precipitation in pentane followed by filtration and subsequently washed with cold pentane. After drying the copolymers under reduced pressure overnight, light blue or nearly white powders were obtained in 60−80% yield, while conversions of SSP were nearly complete based on NMR analyses of resulting block copolymers. ^{1}H NMR spectrum of PNS−PSSP (multiplicity, identity) δ ppm: 6.2−7.3 (b, Ar*H*), 5.9−6.2 (b, −C*H*=C*H*−), 4.0 (b, O−CH_2−CH$_2$), 2.8 (b, −C*H*−CH=CH−C*H*−), 2.5 (b, Ar−CH_2−), 0.6−2.0 (m/b, other C*H* and CH_2).

Membrane Synthesis. In a capped vial, PNS−PSSP (0.4 g) was dissolved into THF (2.0 mL) until a homogeneous solution (clear or slightly opaque) was obtained, and DCPD and/or COE were subsequently added in the solution (stirring for 10 min). To the solution, a mixture of the second-generation Grubbs catalyst (2.5 mg) and THF (0.4 mL) was quickly added and stirred for 10 s. Solution-cast films onto alumina pans (6.5 cm in diameter) were placed in a covered chamber, and the solutions gelled within 5 min. After curing the membranes at RT overnight along with slow THF evaporation and at 90 °C for 1 h, transparent and slightly yellow films were peeled off the substrates and further dried. Base hydrolysis of the PSSP block in the precursor membranes was performed in 30 wt % NaOH in the H_2O/MeOH (5:6) mixture at 70 °C for 48 h. After rinsing the resultant films with DI water several times, the films were soaked in a 20 wt % HCl aqueous solution at room temperature for 24 h. The resultant membranes were washed with DI water and dried at 60 °C under reduced pressure overnight.

Membrane Preparation. Nafion samples were purified according to a procedure reported elsewhere,[45] which included multiple refluxing steps in 3 wt % hydrogen peroxide, DI water, and 1 M sulfuric acid with excessive rinsing after each step. For both Nafion and cross-linked PEMXa films used in this study, samples ∼2.5 × 2.5 cm in size were used for two-electrode (through-plane) proton conductivity and methanol permeability experiments, while samples ∼3 × 0.5 cm were used for swelling and four-electrode (in-plane) proton conductivity experiments.

Proton Conductivity. The proton conductivity of each sample was measured with electrochemical impedance spectroscopy. Membrane resistance was measured at AC frequencies ranging from 100 Hz to 1 MHz using a Solartron impedance system (1260 impedance analyzer, 1287 electrochemical interface, Zplot software). Two-electrode proton conductivity experiments consisted of measuring the resistance of the membrane perpendicular to the plane of the membrane (referred to as through-plane) by sandwiching each film between two stainless steel blocking electrodes. All membranes were immersed in deionized (DI) water for at least 1 week and then quickly removed and enclosed in a sealable Teflon custom-made cell to maintain hydration during impedance measurements. The real impedance was determined from the *x*-intercept of the imaginary versus real impedance data over a high frequency range.[24b] Conductivity values for each sample reported in this study are an average of at least two experiments. Wet membrane thickness (used in the conductivity calculation) was measured after reimmersing each membrane in water. Through-plane conductivity, $\sigma_\perp$, was calculated by

$$\sigma_\perp = \frac{l}{R_\perp A_\perp} \quad (1)$$

where l is the membrane thickness, $R_\perp$ is the resistance (real impedance), and $A_\perp$ is the electrode area (1.22 cm^2).

Four-electrode proton conductivity experiments consisted of measuring the resistance of the membrane along the plane of the membrane (referred to as in-plane), where the resistance was measured between two inner reference electrodes (~1 cm apart) and current applied to the outer electrodes (~3 cm apart) on the surface of the membrane. All membranes were immersed in DI water for more than 1 week prior to being placed in a custom-made four-electrode cell. The cell applied the appropriate pressure between electrodes and the membrane and had openings that allowed the membrane to be exposed to a controlled environment. The four-electrode cell was then placed in a Tenney chamber with electrical feedthroughs, where resistance was measured as a function of temperature and relative humidity using the same impedance system and frequency ranges as reported for the two-electrode experiments. Experiments were conducted as a function of temperature (ramping up and down in temperature: 30, 40, 60, 80, 70, 50, 30 °C) at two fixed relative humidities: 90 and 50% RH. At each relative humidity, the system was allowed 15 min to ramp to each temperature and then held at that temperature for 5 h. Measurements were only taken when the resistance was constant (at equilibrium) at each condition. At least 10 equilibrium measurements were collected for each sample at each temperature and relative humidity. The in-plane conductivity values reported are the average of these multiple measurements and repeated experiments. The in-plane resistance, $R_{\|}$, or real impedance was determined from the x-intercept of the imaginary versus real impedance data. The in-plane proton conductivity, $\sigma_{\|}$, was calculated by

$$\sigma_{\|} = \frac{d}{R_{\|} A_{\|}} \tag{2}$$

where d is the distance between the reference electrodes (~1 cm) and $A_{\|}$ is the cross-sectional area for conduction (membrane width times thickness). Thicknesses for conductivity experiments were measured directly after each experiment. A schematic diagram of both the two- and four-electrode apparatus and more details regarding the procedures have been documented elsewhere.[24b,51]

Generally, the four-electrode technique (in-plane) is preferred over the two-electrode technique (through-plane) because of the significant frequency dependence on impedance at low frequencies due to interfacial impedance in the latter technique.[52] In this study, impedance measurements with the two-electrode technique were collected at the upper limit of the frequency range, where there is only a minor dependence on frequency.[52] Other investigators have reported ~2.5-fold difference in conductivity for Nafion 117 when comparing the four- and two-electrode techniques.[24b,53] Similar results were obtained in this study for Nafion 117. Despite this difference, the two-electrode technique is of great importance as it measures the membrane impedance in the same direction as methanol transport, which is the direction that is relevant for the direct methanol fuel cell. Also, the values reported here give a magnitude of conductivity required to obtain an adequate voltage response from a direct methanol fuel cell. It is important to note that other investigators have observed an order of magnitude difference (higher) when comparing in-plane to through-plane conductivity for anisotropic sulfonated block copolymers (with lamellar morphology with a preferred orientation in the plane of the membrane). Therefore, great caution should be taken when interpreting conductivity results since numerous publications have reported misleading selectivities (proton conductivity/methanol permeability) with four-electrode conductivity measurements on anisotropic membranes. Although isotropic morphologies were observed in the cross-linked PEMs, only through-plane conductivity measurements were compared to methanol permeability in this study.

Methanol Permeability. Methanol permeability of all samples was measured using a temperature-controlled, side-by-side glass permeation cell (PermeGear, Inc.), where methanol concentration was detected downstream (receptor) with real-time, in-line Fourier transform infrared-attenuated total reflectance (FTIR-ATR) spectroscopy. All experiments were conducted at 25.0 ± 0.1 °C at an upstream (donor) methanol concentration of 2 M, and all samples were saturated in liquid water prior to each experiment. The permeability was determined from the slope of the early time data (downstream methanol concentration versus time). Thicknesses for permeability experiments were measured directly after each experiment. This technique was developed in previous work, and a schematic diagram of the apparatus and details regarding the procedure and permeability calculations have been documented elsewhere.[24]

Water Sorption and Swelling. Water sorption (uptake) was measured according to a procedure detailed elsewhere.[24b] The weights were recorded with a balance (Mettler Toledo, AB54-S) with 0.1 mg accuracy, thicknesses were measured with a micrometer (Mitutoyo) with 1 μm accuracy, and the width and length of all samples were measured with calipers (VWR) with 10 μm accuracy. All sample weights and dimensions were measured for both dry and water-saturated conditions (immersed in liquid water for 3 weeks). Changes were calculated on a dry basis, where weight uptake was determined by

$$\text{wt } \% = \frac{m_{\text{wet}} - m_{\text{dry}}}{m_{\text{dry}}} \times 100 \tag{3}$$

where m_{wet} and m_{dry} are the wet and dry weight of the membrane, respectively. Swelling (e.g., thickness change) was determined by

$$\text{swelling } \% = \frac{l_{\text{wet}} - l_{\text{dry}}}{l_{\text{dry}}} \times 100 \tag{4}$$

where l_{wet} and l_{dry} are the wet and dry thicknesses of the membrane, respectively. For thickness measurements, ~5−10 readings at different positions on the membrane were collected, while width and length measurements consisted of five and three readings, respectively, at different positions. A minimum of two samples were used for each sorption and swelling experiment. These changes in weights and dimensions from dry to water-saturated states are listed in Table 1, where the average and standard deviation of all the measurements (different positions and samples) are reported. The thickness used to calculate other values, such as conductivity and permeability, was only that of the specific membrane of the experiment.

Acknowledgment. This work was supported by the U.S. Department of Energy through Grant 5-35908 and the Abu Dhabi-Minnesota Institute for Research Excellence (ADMIRE); a partnership between the Petroleum Institute (PI) of Abu Dhabi and the Department of Chemical Engineering and Materials Science of the University of Minnesota. Use of the Advanced Photon Source at Argonne National Laboratories was supported by the US DOE under Contract W-31-109-Eng-38. Parts of this work were carried out in the University of Minnesota I.T. Characterization Facility, which receives partial support from NSF through the NNIN program. The authors acknowledge the financial support of the National Science Foundation (CAREER 0644593; IGERT 0221664) and the U.S. Army Research Office (W911NF-05-1-0036). We thank Louis Pitet for acquiring the Synchrotron SAXS data.

Supporting Information Available: Table S1 and Figures S1−S12 containing supporting NMR, IR, SEC, SAXS, DSC, XPS, conductivity, and tensile test data. This material is available free of charge via the Internet at http://pubs.acs.org.

References and Notes

(1) Carrette, L.; Friedrich, K. A.; Stimming, U. *ChemPhysChem* **2000**, *1*, 162–193.
(2) Wasmus, S.; Kuver, A. *J. Electroanal. Chem.* **1999**, *461*, 14–31.
(3) Olah, G. A.; Goeppert, A.; Prakash, G. K. S. *Beyond Oil and Gas: The Methanol Economy*; Wiley-VCH: New York, 2006.
(4) Smitha, B.; Sridhar, S.; Khan, A. A. *J. Membr. Sci.* **2005**, *259*, 10–26.
(5) Mauritz, K.; Moore, R. *Chem. Rev.* **2004**, *104*, 4535–4585.
(6) (a) Hsu, W. Y.; Gierke, T. D. *Macromolecules* **1982**, *15*, 101–105. (b) Schmidt-Rohr and, K.; Chen, Q. *Nat. Mater.* **2008**, *7*, 75–83.
(7) (a) Ravikumar, M. K.; Shukla, A. K. *J. Electrochem. Soc.* **1996**, *143*, 2601–2606. (b) Heinzel, A.; Barragan, V. M. *J. Power Sources* **1999**, *84*, 70–74.
(8) (a) Rikukawa, M.; Sanui, K. *Prog. Polym. Sci.* **2000**, *25*, 1463–1502. (b) Kreuer, K. D. *J. Membr. Sci.* **2001**, *185*, 29–39. (c) Li, Q.; He, R.; Jensen, J. O.; Bjerrum, N. J. *Chem. Mater.* **2003**, *15*, 4896–4915. (d) Hickner, M. A.; Ghassemi, H.; Kim, Y. S.; Einsla, B. R.; McGrath, J. E. *Chem. Rev.* **2004**, *104*, 4587–4612. (e) Hicker, M. A.; Pivovar, B. S. *Fuel Cells* **2005**, *5*, 213–229. (f) Souzv, R.; Ameduri, B. *Prog. Polym. Sci.* **2005**, *30*, 644–687. (g) Deluca, N. W.; Elabd, Y. A. *J. Polym. Sci., Part B: Polym. Phys.* **2006**, *44*, 2201–2225. (h) Neburchilov, V.; Martin, J.; Wang, H.; Zhang, J. *J. Power Sources* **2007**, *169*, 221–238.
(9) Carretta, N.; Tricoli, V.; Picchioni, F. *J. Membr. Sci.* **2000**, *166*, 189–197.
(10) (a) Yin, Y.; Fang, J.; Cui, Y.; Tanaka, K.; Kita, H.; Okamoto, K. *Polymer* **2003**, *44*, 4509–4518. (b) Park, H. B.; Lee, C. H.; Sohn, J. Y.; Lee, Y. M.; Freeman, B. D.; Kim, H. J. *J. Membr. Sci.* **2006**, *285*, 432–443. (c) Endo, N.; Matsuda, K.; Yaguchi, K.; Hu, Z.; Chen, K.; Higa, M.; Okamoto, K. *J. Electrochem. Soc.* **2009**, *156*, B628–B633.
(11) Guo, Q. H.; Pintauro, P. N.; Tang, H.; O'Connor, S. *J. Membr. Sci.* **1999**, *154*, 175–181.
(12) Xiao, L.; Zhang, H.; Scanlon, E.; Ramanathan, L. S.; Choe, E.-W.; Rogers, D.; Apple, T.; Benicewicz, B. C. *Chem. Mater.* **2005**, *17*, 5328–5333.
(13) Schuster, M.; de Araujo, C. C.; Atanasov, V.; Andersen, H. T.; Kreuer, K. D.; Maier, J. *Macromolecules*, in press.
(14) Miyatake, K.; Chikashige, Y.; Higuchi, E.; Watanabe, M. *J. Am. Chem. Soc.* **2007**, *129*, 3879–3887.
(15) (a) Lee, H.-S.; Roy, A.; Lane, O.; McGrath, J. E. *Polymer* **2008**, *49*, 5387–5396. (b) Kim, D. S.; Robertson, G. P.; Kim, Y. S.; Guiver, M. D. *Macromolecules* **2009**, *42*, 957–963. (c) Yu, X.; Roy, A.; Dunn, S.; Badami, A. S.; Yang, J.; Good, A. S.; McGrath, J. E. *J. Polym. Sci., Part A: Polym. Chem.* **2009**, *47*, 1038–1051. (d) Nakabayashi, K.; Matsumoto, K.; Higashihara, T.; Ueda, M. *J. Polym. Sci., Part A: Polym. Chem.* **2008**, *46*, 7332–7341. (e) Roy, A.; Hickner, M. A.; Yu, X.; Li, Y.; Glass, T. E.; McGrath, J. E. *J. Polym. Sci., Part A: Polym. Chem.* **2006**, *44*, 2226–2239.
(16) (a) Bates, F. S.; Fredrickson, G. H. *Phys. Today* **1999**, 32–38. (b) Ruzette, A.-V.; Leibler, L. *Nat. Mater.* **2005**, *4*, 10–31.
(17) (a) Wang, H.; Capuano, G. A. *J. Electrochem. Soc.* **1998**, *145*, 780–784. (b) Shen, M.; Roy, S.; Kuhlmann, J. W.; Scott, K.; Lovell, K.; Horsfall, J. A. *J. Membr. Sci.* **2005**, *251*, 121–130.
(18) (a) Ding, J.; Chuy, C.; Holdcroft, S. *Chem. Mater.* **2001**, *13*, 2231–2233. (b) Ding, J.; Chuy, C.; Holdcroft, S. *Adv. Funct. Mater.* **2002**, *12*, 389–394. (c) Yang, Y.; Holdcroft, S. *Fuel Cells* **2005**, *2*, 171–186.
(19) (a) Norsten, T. B.; Guiver, M. D.; Murphy, J.; Astill, T.; Navessin, T.; Holdcroft, S.; Frankamp, B. L.; Rotello, V. M.; Ding, J. *Adv. Funct. Mater.* **2006**, *16*, 1814–1822. (b) Nieh, M.-P.; Guiver, M. D.; Kim, D. S.; Ding, J.; Norsten, T. *Macromolecules* **2008**, *41*, 6176–6182.
(20) Zhai, M.; Chen, J.; Hasegawa, S.; Maekawa, Y. *Polymer* **2009**, *50*, 1159–1165.
(21) Zhang, Z.; Chalkova, E.; Fedkin, M.; Wang, C.; Lvov, S. N.; Komarneni, S.; Chung, T. C. M. *Macromolecules* **2008**, *41*, 9130–9139.
(22) Tsang, E. M. W.; Zhang, Z.; Shi, Z.; Soboleva, T.; Holdcroft, S. *J. Am. Chem. Soc.* **2007**, *129*, 15106–15107.
(23) Kim, J.; Kim, B.; Jung, B. *J. Membr. Sci.* **2002**, *207*, 129–137.
(24) (a) Elabd, Y. A.; Napadensky, E.; Sloan, J. M.; Crawford, D. M.; Walker, C. W. *J. Membr. Sci.* **2003**, *217*, 227–242. (b) Elabd, Y. A.; Beyer, F. L.; Walker, C. W. *J. Membr. Sci.* **2004**, *231*, 181–188. (c) Elabd, Y. A.; Napadensky, E.; Walker, C. W.; Winey, K. I. *Macromolecules* **2006**, *39*, 399–407.
(25) Serpico, J. M.; Ehrenberg, S. G.; Fontanella, J. J.; Jiao, X.; Perahia, D.; McGrady, K. A.; Sanders, E. H.; Kellogg, G. E.; Wnek, G. E. *Macromolecules* **2002**, *35*, 5916–5921.
(26) Shi, Z.; Holdcroft, S. *Macromolecules* **2005**, *38*, 4193–4201.
(27) Park, M. J.; Downing, K. H.; Jackson, A.; Gomez, E. D.; Minor, A. M.; Cookson, D.; Weber, A. Z.; Balsara, N. P. *Nano Lett.* **2007**, *7*, 3547–3552.
(28) Chen, L.; Phillip, W. A.; Cussler, E. L.; Hillmyer, M. A. *J. Am. Chem. Soc.* **2007**, *129*, 13786–13787.
(29) Okamura, H.; Takatori, Y.; Tsunooka, M.; Shirai, M. *Polymer* **2002**, 3155–3162.
(30) Lienkamp, K.; Ruthard, C.; Lieser, G.; Berger, R.; Groehn, F.; Wegner, G. *Macromol. Chem. Phys.* **2006**, *207*, 2050–2065.
(31) Chen, L.; Hillmyer, M. A. *Macromolecules*, **2009**, *42*, 4237−4243.
(32) Lienkamp, K.; Schnell, I.; Groehn, F.; Wegner, G. *Macromol. Chem. Phys.* **2006**, *207*, 2066–2073.
(33) Wang, J.-S.; Matyjaszewski, K. *J. Am. Chem. Soc.* **1995**, *117*, 5614–5615.
(34) In related studies we have found that a minimum number of reactive norbornene groups per polymer chain is needed for effective cross-linking with the matrix phase.
(35) Aylward, N. N. *Polym. Lett.* **1970**, *8*, 377–380.
(36) Scholl, M.; Ding, S.; Lee, C. W.; Grubbs, R. H. *Org. Lett.* **1999**, *1*, 953–956.
(37) Teubner, M.; Strey, R. *J. Chem. Phys.* **1987**, *87*, 3195–3200.
(38) Schubert, K.-V.; Strey, R.; Kline, S. R.; Kaler, E. W. *J. Chem. Phys.* **1994**, *101*, 5343–5355.
(39) Pernot, H.; Baumert, M.; Court, F.; Leibler, L. *Nat. Mater.* **2002**, *1*, 54–58.
(40) Liu, D.; Kyriakides, S.; Case, S. W.; Lesko, J. J.; Li, Y.; McGrath, J. E. *J. Polym. Sci., Part B: Polym. Phys.* **2006**, *44*, 1453–1465.
(41) (a) Park, M. J.; Nedoma, A. J.; Geissler, P. L.; Balsara, N. P.; Jackson, A.; Cookson, D. *Macromolecules* **2008**, *41*, 2271–2277. (b) Park, M. J.; Balsara, N. P. *Macromolecules* **2008**, *41*, 3678–3687.
(42) Elabd, Y. A.; Napadensky, E. *Polymer* **2004**, *45*, 3037–3043.
(43) Hsu, W. Y.; Barkley, J. R.; Meakin, P. *Macromolecules* **1980**, *13*, 198–200.
(44) Tang, H.; Pintauro, P. N. *J. Appl. Polym. Sci.* **2001**, *79*, 49–59.
(45) Hallinan, D. T. Jr; Elabd, Y. A. *J. Phys. Chem. B* **2007**, *111*, 13221–13230.
(46) Kopitzke, R. W.; Linkous, C. A.; Anderson, H. R.; Nelson, G. L. *J. Electrochem. Soc.* **2000**, *147*, 1677–1681.
(47) Halim, J.; Buchi, F. N.; Haas, O.; Stamm, M.; Scherer, G. G. *Electrochim. Acta* **1994**, *39*, 1303–1307.
(48) Chen, H.; Palmese, G. R.; Elabd, Y. A. *Chem. Mater.* **2006**, *18*, 4875–4881.
(49) DeLuca, N. W.; Elabd, Y. A. *J. Power Sources* **2006**, *163*, 386–391.
(50) Schmidt, S. C.; Hillmyer, M. A. *Macromolecules* **1999**, *32*, 4794–4801.
(51) DeLuca, N. W.; Elabd, Y. A. *J. Membr. Sci.* **2006**, *282*, 217–224.
(52) Cahan, B. D.; Wainright, J. S. *J. Electrochem. Soc.* **1993**, *140*, L185–L186.
(53) (a) Gardner, C. L.; Anantaraman, A. V. *J. Electroanal. Chem.* **1995**, *395*, 67–73. (b) Fontanella, J. J.; McLin, M. G.; Wintersgill, M. C.; Calame, J. P.; Greenbaum, S. G. *Solid State Ionics* **1993**, *66*, 1–4. (c) Pourcelly, G.; Oikonomous, A.; Gavach, C.; Hurwitz, H. D. *J. Electroanal. Chem.* **1990**, *287*, 43–49.
(54) Phillip, W. A.; Martono, E.; Chen, L.; Hillmyer, M. A.; Cussler, E. L. *J. Membr. Sci.* **2009**, *337*, 39–46.
(55) Cenyowa, J. *Polymer* **1978**, *19*, 73–76.